Distinguishing Modes of Eukaryotic Gradient Sensing

R. Skupsky,*[†] W. Losert,[†] and R. J. Nossal*

*Laboratory of Integrative and Medical Biophysics, National Institute of Child Health and Human Development, National Institutes of Health, Bethesda, Maryland 20892; and [†]Department of Physics, University of Maryland, College Park, Maryland 20742

ABSTRACT   We develop a mathematical model of phosphoinositide-mediated gradient sensing that can be applied to chemotactic behavior in highly motile eukaryotic cells such as *Dictyostelium* and neutrophils. We generate four variants of our model by adjusting parameters that control the strengths of coupled positive feedbacks and the importance of molecules that translocate from the cytosol to the membrane. Each variant exhibits a qualitatively different mode of gradient sensing. Simulations of characteristic behaviors suggest that differences between the variants are most evident at transitions between efficient gradient detection and failure. Based on these results, we propose criteria to distinguish between possible modes of gradient sensing in real cells, where many biochemical parameters may be unknown. We also identify constraints on parameters required for efficient gradient detection. Finally, our analysis suggests how a cell might transition between responsiveness and nonresponsiveness, and between different modes of gradient sensing, by adjusting its biochemical parameters.

INTRODUCTION

Many eukaryotic cells respond with directional movement to spatial and/or temporal gradients of small molecules that bind to cell surface receptors. This process, called chemotaxis, is important in phenomena as diverse as the immune response of higher animals, wound healing, neuronal patterning, vascular, and embryonic development (1–5), as well as the food gathering and social behavior of some ameboid cells (6). Gradient sensing is the aspect of chemotaxis whereby cells transduce the external distribution of chemotactic ligand into an internal distribution of signaling molecules that effect the morphological and mechanical changes necessary for movement (7). In this article we focus on gradient sensing in highly motile cells such as neutrophils and the aggregating slime-mold, *Dictyostelium discoideum*. These cells respond with directional movement to differences in ligand concentration of a few percent across their length with cellular velocities of order of 10 μm/min (approximately one cell length per minute), over several orders of magnitude in absolute concentration (8,9).

Phosphoinositides in gradient sensing

Recent experiments in both *Dictyostelium* and neutrophils have suggested that phosphoinositide (PI) signaling at the plasma membrane mediates gradient sensing in these cells by localizing molecules that relay signals from receptor activation to cytoskeletal rearrangements (10,11). PIs are signaling lipids that are phosphorylated by kinases, and dephosphorylated by phosphatases, at different positions on their inositol headgroup. Depending on their phosphorylation state, PIs can recruit specific molecules from the cytosol to the membrane, including those that affect cellular movement and those that affect their own interconversion (12,13). The feedback regulation and membrane localization of PIs make them well suited to mediate cell surface processes that require highly localized and amplified signals in space and time, such as chemotaxis. In particular, 3′PIs (PIs that are phosphorylated in the 3′ position) are thought to play a causal role in nucleating the actin-based protrusions necessary for cell movement, and markers for their production show qualitatively similar dynamics to actin polymerization in chemotaxing cells (14–16). These markers show similar dynamics as well in cells that are round and cannot form protrusions due to treatment with actin depolymerizing agents (17,18), suggesting that aspects of gradient sensing may be decoupled from the morphological and mechanical events involved in chemotaxis.

Recent models relating to PI-mediated gradient sensing

The suggestion that gradient sensing can be decoupled from motility, and that it is mediated by a feedback scheme such as those implicated in PI signaling, has inspired several recent mathematical models. Each accounts for characteristic behaviors in a different way. Levchenko and Iglesias (21) have analyzed a general model that maps onto a scheme of receptor-mediated production of phosphatidylinositol (3,4,5) tris-phosphate (PI(3,4,5)P$_3$) with feedback through small GTPases (henceforth referred to as the LI model). Narang et al. (22) have analyzed a model abstracted from a scheme of receptor-mediated regulation of phosphatidylinositol (4,5)

Abbreviations used: PI, phosphatidylinositol/phosphoinositide; 3′PI, PI phosphorylated in the 3′ position; PI(3,4,5)P$_3$, PI(3,4,5) tris-phosphate; PI(4,5)P$_2$, PI(4,5) bis-phosphate; PI(3,4)P$_2$, PI(3,4) bis-phosphate; PI3K, PI 3′kinase; PLC, phospholipase C; HTG, heterotrimeric G-protein; gP, small GTPase; GEF, GTP exchange factor; GTP, guanosine 5′-triphosphate; GDP, guanosine 5′-biphosphate; PITP, PI transfer protein; PIPK, PI(4)P 5′kinase; GAP, GTPase activating protein; subscripts c/m/0, cytosolic/membrane/total for a given molecule.

bis-phosphate ($PI(4,5)P_2$) levels, modulated by phospholipase C (PLC) activity and feedback through substrate delivery from other membrane compartments (henceforth, NSL model). Postma and Van Haastert (23) have analyzed a general model in which a cytosolic effector molecule enhances receptor-mediated production of a lipid second messenger that, in turn, recruits the effector molecule from the cytosol to the membrane (henceforth, PvH model). These models share important features with our model; other recent models take substantially different approaches (see, for example, Rappel et al. (19) and Haugh and Schneider (20)).

In addition to being based on different biochemical schemes, the above models demonstrate qualitative differences in behavior, suggesting that they represent different modes of gradient sensing. For example, in the LI model the steady-state response of the cell always reflects the current stimulus, whereas in the NSL model, once elicited, a cellular response can persist independently of the external stimulus under some conditions. The PvH model requires a high baseline concentration of translocating molecule on the membrane for efficient gradient sensing. Qualitative comparisons of these models, addressing some of these differences, are published in several recent reviews (7,24).

Our model

If the gradient sensing machinery of the cell is modeled as a reaction-diffusion system, we expect to find qualitative differences in systems that include different spatial couplings and/or exhibit different types of bifurcations. Indeed, a general picture of PI signaling suggests that the existence of coupled positive feedbacks and/or cooperative interactions can lead to bifurcations; molecules that translocate to the membrane from a shared pool in the cytosol can affect spatial couplings. To our knowledge, a systematic and quantitative analysis of how these elements lead to qualitative differences in gradient sensing behavior (such as those noted above), has not been done.

To this end we develop a mathematical model of PI-mediated gradient sensing at an intermediate level of detail. Our model consists of a set of reaction-diffusion equations for the spatiotemporal patterns of 3′PIs on the plasma membrane, as well as for the kinase that generates them and the phosphatase that deactivates them. It reproduces much of the translocation dynamics observed experimentally in *Dictyostelium*.

By appropriately adjusting parameters, we generate four variants of our model. Our model variants differ in whether coupled positive feedbacks lead to multiple steady states, and whether redistribution of translocating molecules plays an essential role in amplifying responses to gradients; they illustrate the qualitatively different modes of gradient sensing that result in each case.

Distinguishing modes of gradient sensing

Each of our model variants demonstrates three characteristic gradient sensing behaviors, which are enumerated in the next section. We find that differences between the variants become evident in simulated dose-response experiments that highlight transitions between efficient and inefficient gradient sensing. These results are used to define criteria that distinguish between the ''modes'' of gradient sensing illustrated by our model variants. Applying these criteria to analyze the parameter space of our model suggests that boundaries between different types of behavior can be sharp, and regions that display a given behavior can be narrow with respect to variation of some combinations of parameters. Thus, efficient gradient sensing might require homeostatic mechanisms that regulate combinations of parameters to be within specified ranges. Further, because cells in a given population will have a distribution of biochemical parameters, we expect that subpopulations might function in different regions of parameter space, making use of different modes of gradient sensing. Finally, because biochemical parameters can vary during the course of development (e.g., through changes in gene expression), any given cell might transition between efficient and inefficient gradient sensing, and between different modes of gradient sensing, to suit its needs.

MODEL DEVELOPMENT

Characteristic behaviors

A mathematical model of eukaryotic gradient sensing should reproduce three characteristic behaviors, which can be seen in the dynamics of markers for 3′PIs on the plasma membrane:

1. Cells adapt to the average concentration of ligand in solution. This allows sensitivity to relative gradients over many orders of magnitude in absolute concentration (9,25). In the particular case where a uniform dose of ligand is applied suddenly, the cellular response is transient and returns to baseline (26).
2. When exposed to a shallow and static gradient of ligand, the cell responds with a sharp and persistent internal gradient of signaling molecules (27). This permits immune cells to migrate toward a source of infection and amoeboid cells to move toward a food source over long distances.
3. If the gradient of ligand changes direction, the distribution of signaling molecules will follow with some fidelity (18). A neutrophil thereby can capture a moving bacterium, and *Dictyostelium* cells can form dynamic patterns during development in response to changing gradients of cAMP.

Conceptual framework: local activation/global inhibition

The above behaviors suggest that gradient sensing is mediated by a balance of molecules that act locally, and those that act globally. The former generate a strong response to the

greater stimulus at the front of a cell in a gradient (a local quantity), whereas the latter mediate adaptation to the average stimulus (a global quantity). This observation is often summarized as ''local activation, global inhibition'' (31,32). The equations written to describe such systems (including our own) generally share important features with the activator/inhibitor models developed by Meinhardt and Geirer to explain patterning in development (29), which were extended by Meinhardt to explain aspects of chemotactic response (30).

Geometry and space/timescales

We treat the cell as a disk with the cytosol as its interior and the plasma membrane as its perimeter, reflecting the geometry of a rounded cell where actin has been depolymerized. X marks the position along the membrane and is normalized so that the circumference of the cell is 1. Cytosolic molecules translocate to this boundary, along which 3′PIs diffuse (Fig. 1). Although more pattern forming possibilities would be available if, for example, we treated the membrane as two-dimensional, this simplified geometry adequately accounts for the gradient sensing possibilities that we investigate.
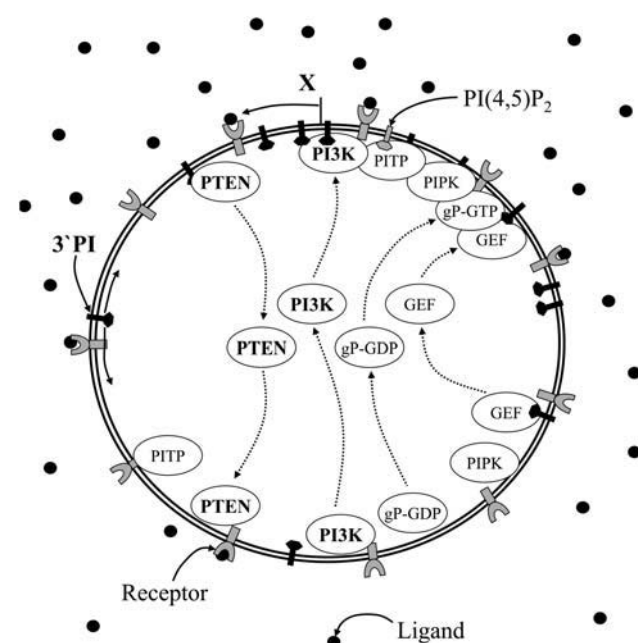

FIGURE 1   Schematic of the model. The plasma membrane is modeled as the perimeter of a circle, parameterized by the normalized coordinate, X, along which 3′PIs diffuse and to which cytosolic molecules translocate. Translocation dynamics depicted at the top of the circle occur at the leading edge of a cell in a gradient of stimulus, or transiently in response to a uniform step stimulus. Dynamics depicted at the bottom occur at the back of a cell in a gradient, or during adaptation to a uniform stimulus. Dynamics of molecules labeled in bold type are calculated explicitly in our model; those in normal font are set to steady-state values with respect to those modeled, and those in gray are held fixed. Abbreviations are listed in the ''Abbreviations used'' footnote at the beginning of the article. The schematic does not include all processes modeled.

A rounded *Dictyostelium* cell might have a radius (r_c) of 4 μm, and the fastest cellular responses occur on timescales of seconds (17,18). Diffusion coefficients for cytosolic proteins, membrane bound proteins, and membrane lipids, might be of order 20 μm^2/s, 0.03 μm^2/s, and 0.5 μm^2/s, respectively (33–35). On cellular length scales, these estimates result in diffusion times of order 100 ms, 100 s, and 1 s, respectively ($t \sim r_c^2/2dD$, where d is the dimension of the space and D is the relevant diffusion coefficient). Due to these differences in timescales, we simplify our model by treating cytosolic molecules as being uniformly distributed and membrane bound proteins as fixed. Lipid diffusion, however, occurs on the same timescale as cellular response and is calculated. Thus, in our model, cytosolic molecules act globally, coupling reactions at all points on the membrane, proteins act locally, and the spatial characteristics of lipids are context dependent. For a contrasting interpretation, see the model of Rappel et al. (19) where delays due to cytosolic diffusion play an essential role.

Coupling to outside stimuli

In both *Dictyostelium* and neutrophils, ligand binding activates receptors, which activate the heterotrimeric G-proteins (HTGs) to which they are coupled, in a pattern that closely reflects that of ligand in solution (18,34,36). Both receptor and HTG activation drive recruitment and activation of type I PI3′ kinases (PI3Ks, which are enzymes that phosphorylate PIs in the 3′ position), though many details are unknown (37,38). For these reasons and because, at least in *Dictyostelium*, receptor and HTG desensitization do not seem to drive adaptation on timescales considered (39), we let a single variable, $\mathcal{R}$, represent ligand-mediated receptor and HTG activation together, which drive PI3K recruitment and activation. In our model, this defines the external stimulus at each point on the membrane.

Biochemical observations, model variables, and network topology

3′PIs

The 3′PIs thought to be relevant in gradient sensing are PI(3,4,5)P$_3$ and PI(3,4)P$_2$, both of which comprise on the order of 0.02% of total plasma membrane lipid in resting cells and specifically act to recruit a similar set of cytosolic molecules to the membrane (40–42). Production of PI(3,4,5)P$_3$ by PI3K acting on PI(4,5)P$_2$, and of PI(3,4)P$_2$ by dephosphorylation of PI(3,4,5)P$_3$, are thought to be the relevant production pathways (40,43). In addition, there is evidence in neutrophil-like cell lines for a positive feedback from 3′PIs to delivery of PI(4,5)P$_2$ to PI3K, involving small GTPases of the Arf and Rho family (44–46). This is highlighted by Loop I in Fig. 2.

PI(3,4)P$_2$ dynamics generally follows PI(3,4,5)P$_3$ dynamics with a slight lag (47). However, there is evidence in
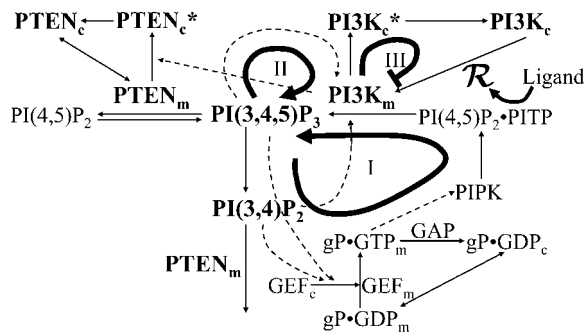
FIGURE 2 Biochemical scheme. Numbered feedback loops highlight a suggested network topology. Solid arrows denote chemical conversions, whereas dashed arrows denote stimulation/activation. Loops I and II, representing positive feedbacks, constitute an amplification module; $\mathcal{R}$ represents the outside stimulus that drives this module by stimulating PI3K translocation to the membrane. Negative feedback Loop III, representing PI3K phosphorylation and inactivation, accounts for response adaptation. Subscripts m and c denote membrane-bound and cytosolic, respectively, and * denotes phosphorylated species, which are catalytically inactive in our model. Abbreviations and fonts are used as in Fig. 1.

Dictyostelium cells suggesting that disruption of a phosphatase that acts on both (PTEN, discussed below) affects their dynamics differently (48). Thus, we model PI(3,4,5)P$_3$ and PI(3,4)P$_2$ separately, and use the scaled variables, P_3 and P_2, to represent their concentrations. Their sum, which we denote P_n, is a primary output of our model.

Membrane bound PI3K and PTEN

The enzyme that generates 3′PIs, a PI3K, and an enzyme that dephosphorylates them, the PTEN phosphatase, are also essential components of our model. As mentioned, PI3K localization and activation are thought to be coupled to outside stimuli. Further, PI3K localization in *Dictyostelium* seems to parallel 3′PI localization upon cellular stimulation (37). If we consider 3′PIs to be the primary signal that localizes other molecules in gradient sensing, this suggests a positive feedback from 3′PIs to the enzymes that produce them, represented by Loop II in Fig. 2. PTEN translocation to the membrane occurs in a pattern inverse to that of PI3K in *Dictyostelium* (37,49). This amplifies the effects of Loop II. In our model, the variables K_m and T_m represent scaled concentrations on the membrane of PI3K and PTEN, respectively.

Cytosolic/inactive PI3K and PTEN

Because cellular response eventually adapts to the average stimulus, as do PI3K and PTEN activities (37,49), some form of integral feedback regulation must exist (50). We represent this by negative feedback Loop III in Fig. 2. Both PI3K and PTEN activity are known to be controlled by phosphorylation in some cell types (51,52). We use the scaled variables K_c^* and T_c^* to represent the fractional concentrations of PI3K and PTEN, respectively, which are cytoplasmic and phosphorylated. These are catalytically inactive in our model.

Proposed biochemical mechanisms

Loop I: positive feedback through substrate delivery

A possible mechanism for the feedback in Loop I, many elements of which have been studied in neutrophils or neutrophil-like cells, is depicted in Fig. 2. 3′PIs recruit GTP exchange factors (GEFs) to the membrane, where they catalyze the exchange of GDP for GTP in specific small GTPases (g-P) of the Arf and Rho family (53,54). These GTPases are then activated and stabilized on the membrane (55,56), and play roles (together with their regulators) in remodeling the membrane and actin network (57–59). Some have been shown to stimulate PI(4)P5′ kinases (PIPKs) to make additional PI(4,5)P$_2$ (45,46).

Experimental observations do not indicate an accumulation of free PI(4,5)P$_2$ upon cellular stimulation (60,61), suggesting that the PI(4,5)P$_2$ generated by the feedback in Loop I is used immediately. This observation could be explained if the generated PI(4,5)P$_2$ was bound to a transfer protein (PITP) and passed directly to PI3K for conversion to PI(3,4,5)P$_3$ (there is evidence in neutrophils for PITP involvement in PI(3,4,5)P$_3$ production (62)). In our model, we assume this mechanism and do not include the dynamics of free PI(4,5)P$_2$. This simplification is consistent with the lack of clear evidence for spatial gradients of free PI(4,5)P$_2$ in gradient sensing cells (60,63).

Loop II: positive feedback through regulation of enzymatic activity

For the feedback in Loop II, we propose that 3′PIs recruit an as-yet unidentified molecule to the membrane, which stabilizes membrane-bound PI3K. Membrane-bound PI3K then produces more PI(3,4,5)P$_3$. To account for a PTEN dynamic inverse to that of PI3K, we propose that PI3K in its capacity as a protein kinase (64,65), or another molecule whose dynamics parallels PI3K dynamics, phosphorylates PTEN (to our knowledge an interaction between PI3K and PTEN has not yet been directly investigated experimentally). In our model, phosphorylated PTEN is cytosolic and inactive.

Loop III: negative feedback for adaptation

To account for response adaptation, we propose that PI3K on the membrane is phosphorylated by an as-yet unidentified kinase, which is constitutively active on the membrane. Phosphorylated PI3K is cytosolic and inactive in our model. PI3K phosphorylation acts as a mechanism of global inhibition because it depletes the cytosolic pool of active/unphosphorylated PI3K, which is a shared pool for recruitment to the entire membrane.

Assessing the biochemical scheme

Several difficulties, often encountered when modeling cellular signal transduction, need to be confronted in developing our

biochemical scheme. First, the regulatory mechanisms that are necessary to develop our model have not all been studied in, and may not all exist in, a single cell type. In particular, most of the biochemical interactions suggested for Loop I, as well as regulation of PI3K and PTEN by phosphorylation, have been studied in neutrophils, but have not been sufficiently addressed in *Dictyostelium*. On the other hand, the translocation dynamics that our model reproduces have been studied primarily in *Dictyostelium*. Further, several of the relevant biochemical mechanisms, in particular those involved in Loops II and III, are in fact unknown, and the mechanisms that we have proposed are uncertain. In light of these difficulties, we will be primarily concerned in our analysis with the overall roles of coupled positive feedbacks and translocation, and with the differences in gradient sensing mechanism to which they give rise. These types of results should depend on qualitative features of our model, such as network topology, rather than biochemical details. In addition, our model can be used to investigate the consistency of the proposed mechanisms with current data, and to suggest experiments that probe their validity. An example of such an application is outlined below.

Consider the proposed role of PI3K in our model. Recent observations of *Dictyostelium* cells in which 3′PI dynamics have been perturbed suggest that the qualitative features of PI3K and PTEN translocation, in response to a saturating uniform stimulus, remain unchanged under these conditions (37,48,66). We have simulated the response of our model under conditions of PI3K inhibition and still found a substantial PI3K translocation to the membrane in response to large uniform stimuli, in accordance with these experimental observations (though the magnitude is slightly less and the time course slightly faster; results not shown). More significant differences in translocation dynamics, between conditions where PI3K is inhibited and where it is not, are found in responses to gradients and/or weaker stimuli. Responses to these types of stimuli should be investigated experimentally to further probe a possible involvement of PI3K activity in regulating translocation dynamics.

To reproduce the PTEN translocation observed in *Dictyostelium* cells where PI3K is inhibited, however, our model must be extended to include PI3K-independent regulation of PTEN (or we must assume that another kinase besides

PI3K phosphorylates and inactivates PTEN). Binding to $PI(4,5)P_2$, which might be depleted by phospholipase C (PLC) activity upon cellular stimulation (47,67), is a potential alternative mechanism for regulating PTEN (66,68). Such an extension of our model is the subject of current work.

From the above discussion, it is clear that forms of regulation not included in our biochemical scheme must be relevant for gradient sensing. Thus, our model should be viewed in a more general sense as a module for PI3K-mediated gradient sensing. Under normal conditions, it reproduces the enumerated characteristic responses and the discussed translocation dynamics. However, it must be integrated with models of other biochemical processes to account for cellular response under a wider range of conditions.

Steady-state assumptions and intermediate level of detail

In our model equations, which are presented in the next subsection, we only explicitly consider the variables summarized in Table 1. The spatiotemporal dynamics of the other regulatory molecules in our proposed biochemical scheme are generally less well characterized. Further, to our knowledge, there are no observed delays in cellular response specifically associated with their activation. For these reasons, we introduce the following simplifying procedure concerning these regulatory molecules: kinetic equations are written for their dynamics; time derivatives are set to zero; the resulting steady-state equations are used to express their concentrations in terms of the variables of our model (see Supplementary Material for more details). This procedure has the virtues of preserving steady-state solutions as well as many effects of translocation. Many uncertain biochemical details no longer appear explicitly in our equations, which are often consistent with alternatives that give rise to similar qualitative behaviors. On the other hand, our model parameters are related to real cellular biochemical parameters. Thus, we can investigate how qualitative behaviors depend on these quantities, and whether our biochemical mechanisms are consistent with current data (e.g., our discussion of PI3K inhibition, above). In this way, our model is developed at an intermediate level of detail.

TABLE 1   Model variables and uniform steady-state values in the unstimulated cell

Variable	Meaning	Scaled by	Uniform steady-state values			
			Case 1	Case 2	Case 3	Case 4
$P_n = P_3 + P_2$	Sum of 3′PIs thought to be important in gradient sensing; a primary output of our model	[3′PI] that saturates Loop I; results in the relationship $1/\kappa_m + 1/\kappa_c = 1$ (see Eq. 1a)	0.98	4.0	0.44	2.36
K_m	PI3K on the membrane; generates P_3	A_{cell} [PI3K$_0$]*	0.025	0.064	0.016	0.046
K_c^*	Inactive cytosolic PI3K	A_{cell} [PI3K$_0$]	0.5/A_{cell}	0.5/A_{cell}	0.5/A_{cell}	0.5/A_{cell}
T_m	PTEN on membrane; dephosphorylates 3′PIs	A_{cell} [PTEN$_0$]†	0.1	0.054	0.15	0.071
T_c^*	Inactive cytosolic PTEN	A_{cell} [PTEN$_0$]	0.5/A_{cell}	0.5/A_{cell}	0.5/A_{cell}	0.5/A_{cell}

*[PI3K$_0$] = total PI3K/A_{cell}; A_{cell} is the area of the cell.
†[PTEN$_0$] = total PTEN/A_{cell}.

Scaled equations

Our scaled model equations are based on the biochemical scheme in Fig. 2. They are derived from a more complete set of unscaled equations in Supplementary Material. Linear kinetics have been assumed unless otherwise noted; any more complex terms that appear result from our simplifying steady-state assumptions, and are discussed. Integrals account for exchange of translocating molecules between cytosolic pools and the entire membrane. Because our spatial variable is normalized, these integrals are equivalent to spatial averages (denoted $\langle \, \rangle_X$).

Generally, the parameter χ is used to represent scaled forward rate constants, λ to represent backward rate constants, and κ to represent saturation concentrations and/or concentrations at which a term becomes effective. The parameter ζ is used to represent constitutive processes acting in parallel with the regulated processes of our model. In a lowest order approximation, these constitutive terms account for some of the many processes not included in our model, and for the observation that inhibition of any single process in our model does not generally lead to complete inactivation of the signaling pathway. The biochemical quantities represented by our model parameters are summarized in Table 2. Note that many of our model parameters are combinations of concentrations and rate constants (see Supplementary Material).

3' PI dynamics: a primary model output

The following equations describe the dynamics of the 3'PIs, PI(3,4,5)P$_3$ (P_3), and PI(3,4)P$_2$ (P_2), on the membrane:

$$\frac{\partial P_3}{\partial t} = \chi_3 K_{\mathrm{m}} \left(\frac{\Xi}{1 + K_{\mathrm{m}}/\kappa_3} + \zeta_{3/\mathrm{PITP}} \right) + \zeta_3 - \lambda_3 P_3 (T_{\mathrm{m}} + \zeta_{3/\mathrm{T}})$$
$$+ D \frac{\partial^2 P_3}{\partial X^2}, \tag{1}$$

where

$$\Xi \equiv \frac{P_{\mathrm{n}}}{P_{\mathrm{n}}/\kappa_{\mathrm{m}} + \int_0^1 P_{\mathrm{n}} dX / \kappa_{\mathrm{c}} + 1} + \zeta_{\mathrm{PITP}}, \tag{1a}$$

and

$$P_{\mathrm{n}} \equiv P_3 + P_2; \tag{1b}$$

$$\frac{\partial P_2}{\partial t} = \zeta_2 + \lambda_3 \zeta_{3/\mathrm{T}} P_3 - \lambda_2 P_2 (T_{\mathrm{m}} + \zeta_{2/\mathrm{T}}) + D \frac{\partial^2 P_2}{\partial X^2}. \tag{2}$$

Because the feedbacks in our model generally depend on the sum of the 3'PIs (P_{n}), which is a primary output of our model, we have made the substitution Eq. 1b wherever possible.

In Eq. 1, the term $K_{\mathrm{m}} \Xi / (1 + K_{\mathrm{m}}/\kappa_3)$ accounts for P_3 production due to PI3K acting on PITP-bound PI(4,5)P$_2$. This term couples Loops I and II, and saturates at large K_{m} because the PITP is depleted. The factor Ξ is proportional to the concentration of PITP-bound PI(4,5)P$_2$. Its form (Eq. 1a) is obtained in the Supplementary Material by writing kinetic equations for the molecules in Loop I (see Fig. 2), many of whose spatiotemporal dynamics are not well characterized, and setting their concentrations to steady state with respect to the variables of our model. The denominator of Ξ includes a local term ($P_{\mathrm{n}}/\kappa_{\mathrm{m}}$), which accounts for saturation of this feedback due to depletion of membrane bound molecules, and a global term ($\int_0^1 P_{\mathrm{n}} dX / \kappa_{\mathrm{c}} \equiv \langle P_{\mathrm{n}} \rangle_X / \kappa_{\mathrm{c}}$), which accounts for saturation of this feedback due to depletion of cytosolic molecules that translocate to the membrane (in particular, the

TABLE 2 Model parameters

Parameter	Equation	Interpretation	Value*
χ_3	1	Rate constant for Loop I regulated P_3 production	120.0
κ_{m}		P_{n}, which begins to saturate Loop I by depleting membrane molecules	1.18–5.0
κ_{c}		P_{n}, which begins to saturate Loop I by depleting cytosolic molecules	1.25–6.7
ζ_{PITP}		Rate of gP independent P_3 production/rate constant for gP dependent production	0.025
κ_3		K_{m} at which PI3K binding to PITP·PI(4,5)P2 becomes saturated	0.05
$\zeta_{3/\mathrm{PITP}}$		Rate of PITP independent P_3 production/rate constant for PITP dependent production	0.025
ζ_3		Rate of unregulated P_3 production	0.3
λ_3		Rate constant for P_3 removal by T_{m}	15.0
$\zeta_{3/\mathrm{T}}$		Rate of P_3 conversion to P_2/rate constant for T_{m}-mediated removal.	0.13
ζ_2	2	Rate of unregulated production of P_2	0.02
λ_2		Rate constant for T_{m}-mediated removal of P_2	8.0
$\zeta_{2/\mathrm{T}}$		Rate of unregulated removal of P_2/rate constant for T_{m}-mediated removal	0.05
χ_{K}	3	Rate constant for unregulated K_{c} translocation to the membrane	0.0049–0.0076
$\mathcal{R}$		Ligand-induced, receptor-mediated activation, which drives translocation of K_{c}	External
λ_{K}		Rate constant for K_{m} phosphorylation and removal from the membrane	0.73–4.2
κ_{K}		P_{n} at which 3'PI inhibition of K_{m} return to the cytosol (Loop II) becomes effective	0.95–5.5
χ_{T}	4	Rate constant for T_{c} translocation to the membrane	0.019
λ_{T}		Rate constant for T_{m} phosphorylation by K_{m}	30.0
ζ_{T}		Rate of unregulated T_{m} return to cytosol/rate constant for T_{m} phosphorylation by K_{m}	0.002
$\lambda_{\mathrm{T}*}$	5	Rate constant for T_{c}^* dephosphorylation in the cytosol	0.15–0.21
$\lambda_{\mathrm{K}*}$	6	Rate constant for K_{c}^* dephosphorylation in the cytosol	0.34–0.58
$\kappa_{\mathrm{K}*}$		K_{c}^* for which the reaction that dephosphorylates PI3K begins to saturate	0.013
D	1, 2	Coefficient of lipid diffusion in units where the circumference of the cell is 1	0.003
A_{cell}	3b, 4a, 5, 6	Area of the cell in units where the circumference is 1 ($1/4\pi$)	$1/4\pi$

*A range is indicated for parameters that differ between the variants. Note that only the parameters κ_{c}, κ_{K}, and γ_0 (see Eq. 7) were used to define the variants; differences in other parameters result from relationships between the parameters. See Supplementary Material for further discussion and specific values.

GEF in Loop I). If the latter term dominates, then under conditions where redistribution of translocating molecule keeps $\langle P_n \rangle_X$ fixed, Ξ will vary approximately linearly with P_n, and hence contain a term linear in P_3. The degradation term in Eq. 1 is linear in P_3, as well. Then, under these conditions, we might expect a sharp change in P_3 production as K_m and T_m vary, and the balance between production and degradation shifts. The terms, ζ_{PITP}, $\zeta_{3/PITP}$, and ζ_3 in Eq. 1 account for constitutive production of P_3, independent of the various molecules in Loop I (see Table 2). The loss terms in Eq. 1 account for dephosphorylation of P_3 at the $3'$ position by PTEN (T_m) and for conversion to P_2 by a phosphatase, such as SHIP (43), whose dynamics are not included in our model ($\zeta_{3/T}$).

Equation 2 describes P_2 dynamics that follows P_3 dynamics with a slight lag. P_2 is generated from P_3 (1st term), as well as from other sources (ζ_2). The loss terms account for dephosphorylation of P_2 at the $3'$ position by PTEN (T_m), and for dephosphorylation by other phosphatases (represented by $\zeta_{2/T}$).

In Eqs. 1 and 2, the relative values of κ_m and κ_c determine the importance of molecules in Loop I that translocate from the cytosol to the membrane; the ratio χ_3/λ_3 is important in determining the strength of Loop I; the ratios D/λ_3 and D/λ_2 control the effects of diffusion on spatial responses. D is the coefficient of lipid diffusion, in units where the circumference of the cell is 1, assumed to be the same for P_3 and P_2.

Membrane bound PI3K: coupling to outside stimuli

To describe the dynamics of membrane bound PI3K (K_m), we write the following equation:

$$\frac{\partial K_m}{\partial t} = \lambda_K \left(\gamma - \frac{K_m}{1 + P_n/\kappa_K} \right), \tag{3}$$

where

$$\gamma \equiv (\chi_K/\lambda_K)(\mathcal{R} + 1)K_c, \tag{3a}$$

and

$$K_c = \left(1 - A_{cell}K_c^* - \int_0^1 K_m dX \right)/A_{cell}. \tag{3b}$$

The term γ in Eq. 3 (defined in Eq. 3a) represents recruitment of cytosolic PI3K (K_c) to the membrane in response to receptor activation by outside stimuli ($\mathcal{R}$). $\mathcal{R}$ is scaled by unregulated recruitment of PI3K to the membrane; the factor $\mathcal{R} + 1$ thus accounts for the sum of receptor-mediated and unregulated recruitment. Equation 3b expresses conservation of total PI3K and is used to eliminate K_c from our equations (total PI3K is scaled to 1); A_{cell} is the area of our two-dimensional model cell, equal to $1/4\pi$ in units where the circumference of the cell is 1. The loss term in Eq. 3 represents PI3K phosphorylation and removal from the membrane by a constitutively active kinase on the membrane, whose concentration is assumed to be fixed and has been absorbed into the scaled parameter, λ_K. The factor $1 + P_n/\kappa_K$ in the denominator accounts for the feedback in Loop II by decreasing the rate of removal of PI3K from the membrane with increasing P_n. Such a factor can be derived by assuming

that $3'$PIs recruit molecules to the membrane that bind stochiometrically to PI3K, preventing PI3K from returning to the cytosol (by stabilizing PI3K on the membrane and inhibiting the kinase that phosphorylates it). The concentration of these molecules, and their complex with PI3K, are set to steady state with respect to our model variables. The fraction of PI3K on the membrane that is free to return to the cytosol is then proportional to $(1 + P_n/\kappa_K)^{-1}$ (derived in the Supplementary Material). This factor becomes important only when $P_n \sim \kappa_K$. Thus, the magnitude of κ_K determines the effectiveness of Loop II in signal amplification.

PTEN dynamics: amplifying the effects of PI3K

The following equations describe the dynamics of PTEN on the membrane (T_m), and of the fraction of total PTEN concentration that is cytosolic and phosphorylated (T_c^*):

$$\frac{\partial T_m}{\partial t} = \chi_T T_c - \lambda_T T_m(K_m + \zeta_T), \tag{4}$$

where

$$T_c = \left(1 - A_{cell}T_c^* - \int_0^1 T_m dX \right)/A_{cell}; \tag{4a}$$

$$\frac{\partial T_c^*}{\partial t} = \lambda_T \int_0^1 T_m K_m dX/A_{cell} - \lambda_{T*}T_c^*. \tag{5}$$

The first term in Eq. 4 accounts for constitutive recruitment of cytosolic PTEN (T_c) to the membrane with rate constant, χ_T. Equation 4a expresses conservation of total PTEN and is used to eliminate T_c from our equations (total PTEN is scaled to 1). The loss term represents PTEN removal from the membrane by PI3K-mediated phosphorylation (K_m), as well as constitutive removal (ζ_T). In Eq. 5, the first term accounts for phosphorylation of PTEN over the entire membrane and subsequent return to the cytosol. The loss term represents dephosphorylation of PTEN in the cytosol, which is constitutive with rate constant λ_{T*}. These equations reproduce a T_m dynamics inverse to K_m dynamics, enhancing the effects of Loop II. Other regulatory mechanisms would have a similar effect if their kinetics paralleled that of PI3K translocation.

Cytosolic/inactive PI3K: adaptation

We write the following equation for the fractional concentration of PI3K that is cytosolic and phosphorylated/inactive (K_c^*):

$$\frac{\partial K_c^*}{\partial t} = \lambda_K \left(\int_0^1 \frac{K_m}{1 + P_n/\kappa_K} \frac{dX}{A_{cell}} - \left(\frac{\lambda_{K^*}}{\lambda_K} \right) \frac{K_c^*}{\kappa_{K^*} + K_c^*} \right). \tag{6}$$

The first term in Eq. 6 represents phosphorylation of PI3K over the entire membrane. We have chosen parameters such that the reaction that dephosphorylates PI3K in the cytosol (2nd term) is saturated ($K_c^* \gg \kappa_{K^*}$). This ensures that, at steady state, we have the following relation (which results from averaging Eq. 3 over the entire membrane, combining

with Eq. 6, and replacing the integral with an equivalent spatial average):

$$\langle\gamma\rangle_X \equiv (\chi_K/\lambda_K)(\langle\mathcal{R}\rangle_X + 1)K_c$$

$$= \left\langle \frac{K_m}{1 + P_n/\kappa_K} \right\rangle_X \sim \frac{A_{cell}\lambda_{K^*}}{\lambda_K} \equiv \gamma_0 = \text{constant}. \quad (7)$$

Thus, adaptation to the average stimulus occurs in our model because PI3K is phosphorylated over the entire membrane, depleting the shared cytosolic pool of unphosphorylated PI3K (K_c), such that γ always return to γ_0 (discussed further below).

Modular structure and driving parameter

Equations 1–5 describe positive feedback (Loops I and II), and can be considered to constitute an amplification module; Eq. 6 represents negative feedback (Loop III), and constitutes an adaptation module. The parameter γ (defined Eq. 3a) is interpreted as a driving parameter. It serves both to couple these modules to each other and to couple the entire system to outside stimuli. The LI model is based on a similar modular structure, as is a more recent variation (69).

This signaling network might function in gradient sensing as follows: receptor activation increases the local value of $\mathcal{R}$, and hence the local value of γ (Eqs. 3 and 3a), recruiting PI3K to the membrane and driving the amplification module (Eqs. 1–5). PI3K on the membrane is then phosphorylated and returns to the cytosol (Eq. 6). The pool of PI3K that is free to return to the membrane (K_c), and hence the value of γ, drops. If $\mathcal{R}$ is uniform, γ returns to γ_0 everywhere (see Eq. 7) and the cellular response returns to baseline. Thus, we interpret γ_0 as setting the baseline state of the cell. If there is a gradient in $\mathcal{R}$, γ will remain elevated at the front of the cell, where $\mathcal{R}$ is above its average value, $\langle\mathcal{R}\rangle_X$. If γ_0 is set appropriately, the amplification module will still be driven in this region, but not at the back of the cell where $\mathcal{R}$ is below $\langle\mathcal{R}\rangle_X$ and γ has dropped below γ_0.

Model variants and parameters

A highly nonlinear response of our amplification module, and the possibility of multiple steady states, is expected if both Loops I and II become strongly activated upon cellular stimulation. If depletion of translocating molecules saturates either of these loops we expect qualitative differences in responses to uniform stimuli and to gradients, where these molecules can redistribute between the front and back of the cell. To investigate these possibilities, we generate four variants of our model by adjusting the parameter κ_K (Eq. 3), which controls the effectiveness of Loop II in signal amplification, and the parameter κ_c (Eqs. 1 and 1a), which controls the degree to which cytosolic depletion saturates Loop I. The resulting differences in the amplification modules of our variants are schematized in Fig. 3. Other model pa-
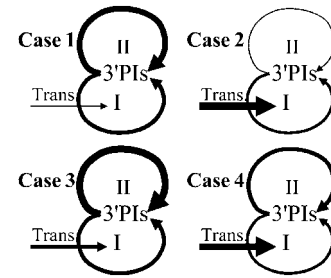

FIGURE 3 Model variants. Depicted elements of the model's amplification module are adjusted to define our model variants; thickness of arrow indicates strength of feature. When Loops I and II are sufficiently activated upon cellular stimulation, coupled positive feedbacks can result in multiple steady states (as in Cases 3 and 4). If translocation (*Trans.*) is important for amplification, then redistribution of molecules between the front and back of the cell can enhance responses to gradients (as in Cases 2 and 4).

rameters have been set empirically to reproduce characteristic responses seen in *Dictyostelium*, as most have not been directly measured.

The uniform steady-state values of our model variables, which are used to initialize our simulations for each variant, may be found in Table 1; parameter values may be found in Table 2; considerations involved in setting them are discussed in the Supplementary Material. Characteristics of our model variants are summarized in Table 3 and discussed below together with relationships to other models in the literature.

Case 1

Coupled positive feedbacks do not result in multiple steady states for any stimulus, and redistribution of signaling molecules does not significantly contribute to response amplification. We expect this variant to share features with the LI model.

TABLE 3 Characteristics of model variants

	Case 1	Case 2	Case 3	Case 4
Relating to coupled positive feedbacks:				
Multiple steady states in response to gradients	No	No	Yes	Yes
Responses to gradients depend on how the stimulus was applied	No	No	Yes	Yes
Highly polarized response to small gradients requires overcoming a stimulus threshold	No	No	Yes	No
Uniform state is unstable to small perturbations	No	No	No	Yes
Relating to translocation:				
Strong responses to uniform stimuli, comparable to responses to gradients	Yes	No	Yes	No
A cytosolic factor is significantly depleted in uniform responses	No	Yes	No	Yes
Redistribution of translocating molecules enhances responses to gradients	No	Yes	Somewhat	Yes

Case 2

Multiple steady states are absent. Upon global stimulation, the amplification module depletes cytosolic molecules, and the response saturates; in response to gradients, however, these molecules are redistributed from the back to the front of the cell, stabilizing and enhancing the polarized response. This variant's amplification module shares features with the PvH model.

Case 3

Coupled positive feedback in Loops I and II is sufficient to produce multiple steady states. The amplification module efficiently amplifies responses to uniform stimuli as well as to gradients, but some redistribution of translocating molecules between the front and back of the cell is necessary to stabilize polarized responses against diffusion. In a shallow gradient of stimulus, the cell can be either in a slightly or highly polarized state; switching between these states requires overcoming a threshold in stimulus. Thus, the steady-state response of the cell depends on the history of the applied stimulus, as well as on its current value. We expect this variant to share features with the NSL model (as well as Meinhardt's formulation, (30)), where strong polarization requires overcoming a stimulus threshold and, under some conditions, cellular responses can persist after the stimulus is removed.

Case 4

As in Case 2, responses to uniform stimuli are weak due to depletion of cytosolic molecules. However, redistribution of translocating molecules in response to a gradient enhances amplification due to coupled positive feedbacks, and results in multiple steady states. The uniform state of the cell is unstable. A slight gradient will induce a highly polarized state, which is stable and can persist when the stimulus is removed. This variant shares features with the NSL and Meinhardt models, as well.

NUMERICAL TECHNIQUES

We converted our system of PDEs to a system of ODEs by discretizing our spatial coordinate with equally spaced points and using a finite difference approximation for diffusion terms. We solved the system using an Euler method, treating diffusive terms in our equations implicitly and reaction parts explicitly (70). The accuracy of our results was checked by varying the time step (h) and number of spatial points (N) by a factor of 2. Deviations between simulations with different h and N were always <0.2% (generally significantly less) for all the patterns of stimulus that were tested.

To characterize polarized distributions of signaling molecules such as P_n, we define the relative polarization as

$$\mathcal{P}\{P_n\} = 2\sqrt{(C\{P_n\})^2 + (S\{P_n\})^2}/\langle P_n \rangle_X, \qquad (8)$$

where $\quad C\{P_n\} \equiv \sum_{j=0}^{N-1} P_n(X_j)\cos(2\pi X_j)$, $S\{P_n\} \equiv \sum_{j=0}^{N-1} P_n(X_j)\sin(2\pi X_j)$, and $\langle P_n \rangle_X \equiv \sum_{j=0}^{N-1} P_n(X_j)/N$. We define the direction of polarization of the distribution as

$$\theta\{P_n\} = \tan^{-1}(S\{P_n\}/C\{P_n\}); \qquad (9)$$

$n\pi$ (n = integer) is added or subtracted appropriately so that θ changes continuously during the course of a simulation. We then define the angular velocity of rotation of the distribution by

$$\mathcal{V}\{P_n\} = \frac{\partial\theta\{P_n\}}{\partial t}. \qquad (10)$$

MODEL CHARACTERIZATION

Amplification modules

The different features of each variant's amplification module (Eqs. 1–5) are depicted in Fig. 3, where the strength or importance of an element is indicated by the thickness of the corresponding arrow. To analyze these differences, we calculate steady-state solutions of Eqs. 1–5 at fixed values of the driving parameter, γ (see Eq. 3a), for each variant. This is equivalent to analyzing the steady-state response of our model without adaptation; the results obtained are suggestive of the differences in response that will be found later when the full system of equations is considered. To further simplify our analysis, we neglect diffusion and make the assumptions that follow concerning the integrals in our equations. As mentioned, these integrals are equivalent to spatial averages.

If the stimulus is uniform then γ will vary uniformly, as will the response of the amplification module; then averages, corresponding to the integrals in our equations, will be equal to their values at any point on the membrane. These solutions are represented by the solid curves in Fig. 4 *a*. Notice that for Cases 2 and 4, due to depletion of cytosolic molecules at higher γ, the steady-state response of the amplification module is less sharp than it is for Cases 1 and 3. The curve for Case 3 shows multiple steady states for a small range of γ, due to the simultaneous activation of Loops I and II. These solid curves suggest differences in the responses of each variant to uniform stimuli, where γ increases transiently and then returns to baseline.

To analyze steady-state responses to nonuniform γ, we fix averages and cytosolic concentrations in our equations at the values determined by the circled points on the solid curves in Fig. 4 *a*. This corresponds to analyzing the response of the amplification module at a single point on the membrane where concentrations everywhere else are held fixed at uniform steady-state solutions for fixed γ (variations at a single point on the membrane will not affect averages or cytosolic concentration). Solutions are represented by the dashed curves in Fig. 4 *a*. Their slope, near their intersections with the solid curves, is an important determinant of steady-state cellular response to a gradient in $\mathcal{R}$ (which generates a
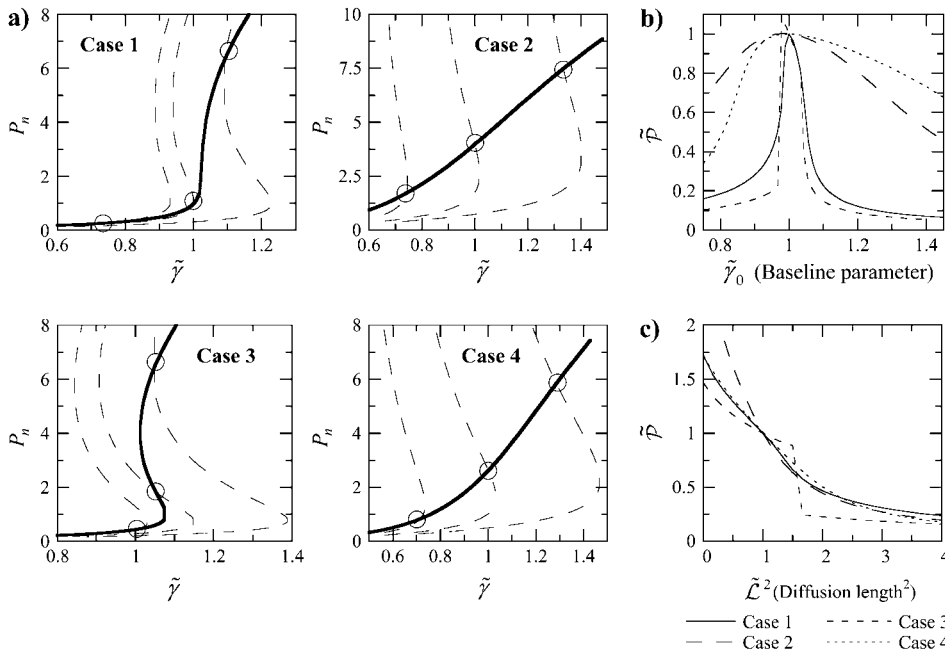
FIGURE 4 (*a*) Amplification modules. Equations 1–5, representing our model's amplification module, are solved for steady state at fixed values of the driving parameter, γ, neglecting diffusion. Solid curves represent uniform responses. Dashed curves represent responses at a single point on the membrane, where other concentrations are held fixed at uniform steady-state values determined by the circled solutions on the solid curves. $\tilde{\gamma} \equiv \gamma/\gamma_i$, $i \in \{1, 2, 3, 4\}$ is the normalized driving parameter, where γ_i is the value of γ_0 that sets the baseline for Case 1 (see Eq. 7). (*b* and *c*) Restrictions on parameters. Steady-state solutions of Eqs. 1–6, calculated with the stimulus given by: $\{\mathcal{R} = 0, (t < 0); \ \mathcal{R} = S + G(1+S)\cos(2\pi X), (t > 0)\}$, where $S = 2$ and $G = 0.05$. $\tilde{\mathcal{P}} \sim \mathcal{P}\{P_n\}$ is the relative polarization of the 3'PI distribution (defined Eq. 8), normalized by the value calculated when all parameters are set at the fixed values used in subsequent simulations (given in Supplementary Material). To investigate restrictions on baseline, $\tilde{\gamma}_0 \equiv \gamma_0/\gamma_i$ is varied (*b*). To investigate restrictions on diffusion length, $\tilde{\mathcal{L}}^2 \equiv \mathcal{L}^2/\mathcal{L}_0^2$ is varied; $\mathcal{L}_0$ is the fixed value of $\mathcal{L}$ used in subsequent simulations (which is the same for all cases) (*c*).

gradient in γ). The dashed curves double back on themselves more strongly for Cases 3 and 4 than they do for Cases 1 and 2. This suggests the possibility of multiple steady states in response to nonuniform γ, resulting from the simultaneous activation of coupled positive feedbacks. For Cases 2 and 4, the solid curves differ from the dashed curves more significantly at their intersections—though the uniform response of the amplification module is relatively weak for these Cases, the response at a point can be quite sharp. This difference reflects the greater importance of translocating molecules in amplifying responses to nonuniform γ.

Constraints on baseline

From the curves in Fig. 4 *a* it is clear that, in order for each variant to reproduce the characteristic behaviors of gradient sensing, there must be different constraints on the baseline state of the cell, as determined by γ_0 (see Eq. 7). If the cell is to adapt to all uniform stimuli, γ_0 should not be set in the bistable region of the solid curves in Fig. 4 *a*. Additionally, if there is to be a sharp cellular response to small gradients in $\mathcal{R}$, γ_0 should be set to a value where response to nonuniform γ, which is approximated without diffusion by the dashed curves in Fig. 4 *a*, is sharp.

To investigate constraints on γ_0, we simulate cellular response to a static, spatially linear gradient in $\mathcal{R}$, using the full set of equations (1–6); γ_0 is varied by appropriately adjusting λ_{K*} and χ_K (see Eq. 7). In Fig. 4 *b*, we plot the normalized polarization that results (see caption), as a function of the normalized baseline parameter, $\tilde{\gamma}_0 \equiv \gamma_0/\gamma_i$;

$i \in \{1, 2, 3, 4\}$ where γ_i is the fixed value of γ_0 for variant i, which is used in subsequent simulations. Note that the values of γ_i have been chosen such that for each curve the polarized response at $\tilde{\gamma}_0 = 1$ is nearly optimal.

For Cases 1 and 3, the peak response in Fig. 4 *b* is constrained to a narrow range of γ. This indicates that for strong responses to relatively weak gradients, γ_0 must be set very near an amplification threshold for the uniform response of the amplification module (compare the positions of the peaks here to the solid curves in Fig. 4 *a*), but robust to perturbations in many other model parameters. The restriction of γ_0 to a narrow range of values suggests that in the development of cells that sense gradients by these mechanisms there must exist homeostatic mechanisms that maintain the baseline state near such a threshold. Levchenko and Iglesias, as well, have found responses to gradients to be sensitive to variations in parameters that set the baseline state of the cell.

Cases 2 and 4, on the other hand, rely on redistribution of signaling molecules between the front and back of the cell to amplify responses to gradients. These cases merely require that γ_0 be high enough for a large fraction of these molecules to be on the membrane in the unstimulated cell (this fraction increases with $\int_0^1 P_n dX = \langle P_n \rangle_X$, which appears in Eqs. 1 and 1a; see also Supplementary Material). Note that for Case 3, the depicted jump in response represents a discontinuity, corresponding to a bifurcation, though only the more polarized steady state is depicted. Postma and Van Haastert have also demonstrated enhanced responses to gradients with a high baseline concentration of translocating molecule on the membrane.

Constraints on diffusion length

Under conditions where Fig. 4 *a* suggests a possible bistable response to some patterns of $\mathcal{R}$, diffusion can destabilize nonuniform steady-state solutions, and cellular response might depend sharply on the relative value of the coefficient of lipid diffusion (D) in our equations. More specifically, steady-state profiles depend on the ratio $\mathcal{L}^2 \equiv D/\lambda$, where λ is a degradation rate constant and $\mathcal{L}^2$ can be thought of as the squared length that a lipid may diffuse before being degraded, per unit concentration of degrading enzyme. Postma and Van Haastert have also analyzed the importance of diffusion length in their model, though it does not include multiple steady states.

In Fig. 4 *c* we vary D, thereby varying $\tilde{\mathcal{L}}^2 \equiv \mathcal{L}^2/\mathcal{L}_0^2$; $\mathcal{L}_0^2$ is the value of $\mathcal{L}^2$ used in subsequent simulations, which was the same for all variants (corresponding to on the order of 5% of the cell's circumference). Again, we plot the normalized polarization of the 3′PI distribution in response to a static gradient, applied such that the more polarized steady state results in cases where multiple steady states are possible. Notice that $\tilde{\mathcal{L}}^2 = 1$ is in the regime where, for each variant, diffusion has a similarly significant effect on the polarized response of the cell. For Case 3, however, the highly polarized state becomes unstable and is abruptly lost as $\tilde{\mathcal{L}}^2$ increases (the discontinuity in the curve represents a bifurcation). Although multiple steady states exist for Case 4 as well, the highly polarized state remains stable, as reflected by the continuous curve.

RESULTS

How well does each model variant account for the characteristic behaviors of gradient sensing, and how might the variants be distinguished? To investigate this we simulate cellular response to uniform stimuli, to static gradients, and to rotating gradients. The full system of equations (Eqs. 1–6) is used, together with the fixed parameter values that define each variant (given in Table 2 and Supplementary Material). Differences between the model variants are seen most clearly in dose-response curves for these simulations, which high-light transitions in cellular response. We use these results to define criteria that distinguish between the modes of gradient sensing illustrated by our model variants.

Uniform stimulus

Fig. 5 *a* illustrates a transient response to a uniform step stimulus applied at $t = 0$. Time courses were qualitatively similar for all cases (Case 4 is depicted). $\mathcal{R}$ is increased suddenly, producing an increase in γ, which then returns to baseline. The concentrations of 3′PIs and PI3K on the membrane (represented by the scaled variables P_n and K_m) increase transiently, whereas the concentration of membrane bound PTEN (T_m) decreases. The peak response, quantified by $(P_n)_{max}$, increases as the size of the step in $\mathcal{R}$ increases, and occurs on a similar timescale to adaptation of γ. The timescale for adaptation increases as the step size decreases, the effect being more pronounced for Cases 1 and 3 than for Cases 2 and 4 (data not shown).

In Fig. 5 *b*, we summarize the results for peak responses to uniform stimuli of magnitude measured by the parameter, S, with a dose-response curve for each variant. Responses are weaker for Cases 2 and 4 than for Cases 1 and 3, due to depletion of cytosolic molecules, consistent with the weaker uniform response of their amplification modules (Fig. 4 *a*, *solid curves*). However, whereas all of the curves show quantitative differences, they are qualitatively similar — continuous and monotonically increasing.

Static gradients

Fig. 6 *a* illustrates the simulated steady-state profile of a cell in a spatially linear gradient of stimulus (Case 4 is depicted, though all of the cases show qualitatively similar profiles). The steady-state relative polarization of the 3′PI distribution for each variant (see Eq. 8), in response to gradients whose strength is measured by the parameter G (see caption), is given in Fig. 6 *b*. Gradients are applied together with, or after adaptation to, a uniform stimulus. All of the variants show a strong relative polarization in response to relatively weak gradients.
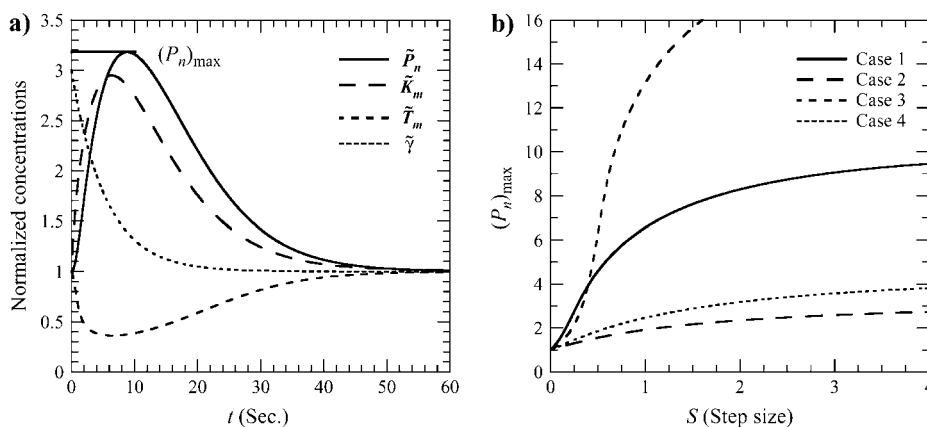

FIGURE 5 Response to a uniform step stimulus applied at $t = 0$: $\{\mathcal{R} = 0$, $(t < 0); \mathcal{R} = S, (t > 0)\}$. (*a*) Sample time course for Case 4, $S = 2$ (time courses for other cases were qualitatively similar). All quantities marked by a tilde are normalized by their values before $t = 0$. (*b*) The normalized peak 3′PI concentration, $(P_n)_{max}$, recorded for each variant as a function of the step size, S, in a dose-response curve.
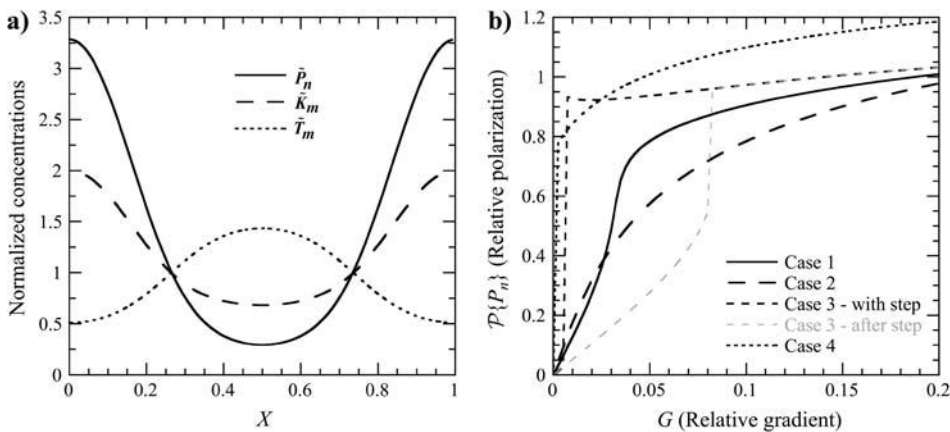
FIGURE 6 Steady-state response to a static, spatially linear gradient. The stimulus is defined by: $\{\mathcal{R} = S_i, \ (t < 0);\ \mathcal{R} = S_f + G(1 + S_f)\cos(2\pi X),\ (t > 0)\}$ where $G = r_c(\partial\gamma/\partial Z)/\langle\gamma\rangle_X$ is a measure of the relative strength of the gradient, $Z = r_c\cos(2\pi X)$ is the coordinate across the cell in the direction of the gradient, and r_c is the radius of the cell. $S_f = 2$; S_i is taken as 0 or 2, depending whether the gradient is applied together with, or after equilibration to, a uniform stimulus (this is only labeled for Case 3, as responses of other cases are independent of S_i). (*a*) Sample profile in a 5% relative gradient ($G = 0.05$). Case 4 is depicted (profiles for all cases were similar). (*b*) The relative polarization of the 3′PI distribution, $\mathcal{P}\{P_n\}$ (defined Eq. 8), recorded for each variant as a function of the relative gradient, G, in a dose-response curve.

For Cases 3 and 4, a discontinuity in the dose-response curve indicates the existence of multiple steady states, highlighting the effects of coupled positive feedbacks, and distinguishing these cases qualitatively from Cases 1 and 2 (the discontinuity for Case 4 is at zero gradient). For Case 3, a threshold in stimulus must be overcome to induce a highly polarized response to small gradients. This is achieved if the gradient is applied together with a sufficient uniform stimulus (*black curve*). Otherwise, the response at small gradients remains weakly polarized (*gray curve*). For Case 4, the uniform state is unstable to arbitrarily small gradients and no such threshold needs to be crossed; other steady-state solutions are not plotted for Case 4.

Rotating gradients

Investigation of responses to rotating gradients (qualitatively investigated experimentally by Parent and Devreotes (32)) may provide insight into the functioning of each variant in natural settings, where stimuli vary in both space and time. To simulate such responses we first applied a static linear gradient together with a uniform step stimulus, and allowed the polarized distribution of signaling molecules to equilibrate. We then began to rotate the gradient at $t = 0$ with different periods of rotation, T. The space/time plots in Fig. 7 *a* record P_n as a grayscale value in sample time courses. The initial gradient is in the direction marked by $X = 0$ and 1 (the normalized spatial variable, X, is periodic); time is measured relative to T (in revolutions); P_n values are normalized by the peak P_n value before gradient rotation.

The first time course, labeled $T = 150$ s, represents cellular response under conditions of slow gradient rotation. The shape of the P_n distribution remains relatively steady, and its direction follows that of the gradient with a slight lag (the grayscale pattern keeps its shape and is translated diagonally with a period of 1). Time courses are qualitatively similar for all cases under these conditions (Case 4 is depicted).

Sample time courses are also given for shorter T, where the model variants demonstrate different kinds of failure in gradient following. For Cases 1 and 2, the polarized distribution becomes gradually washed out; the weakly polarized steady-state distribution that results eventually follows the direction of gradient rotation. Case 3 suddenly becomes depolarized when gradient rotation becomes too fast to follow. Case 4 remains polarized near its initial direction, turning toward the direction of the gradient whenever it is close to the direction of polarization; an oscillatory steady-state behavior results.

For each time course, we calculated the polarization of the 3′PI distribution (Eq. 8) normalized by its value at $t = 0$ ($\tilde{\mathcal{P}}(t)$), and the angular velocity of its direction (Eqs. 9 and 10) normalized by the angular velocity of gradient rotation ($\tilde{\mathcal{V}}(t)$). $\tilde{\mathcal{P}} = 1$ indicates that the polarized distribution remains stable during the gradient rotation; $\tilde{\mathcal{V}} = 1$ indicates that the direction of polarization follows the gradient perfectly (with a slight lag). For each T, we characterize the cellular response by recording the steady-state quantities, $\tilde{\mathcal{P}}_s$ and $\tilde{\mathcal{V}}_s$, which are long-time averages of $\tilde{\mathcal{P}}(t)$ and $\tilde{\mathcal{V}}(t)$, respectively. If no significant oscillations occur, the long-time value of the lag in the direction of polarization, behind that of the gradient, is recorded (θ_L, measured in revolutions, for Cases 1–3). When steady oscillations in $\tilde{\mathcal{P}}(t)$ and $\tilde{\mathcal{V}}(t)$ do occur, the long-time value of the amplitude of oscillations in polarization direction about the average motion is recorded (denoted θ_o, measured in revolutions, for Case 4). Resulting dose-response curves to gradients rotating with different periods are given in Fig. 7 *b*.

For Cases 1 and 2, at shorter T, the P_n distribution becomes increasingly depolarized during an initial transient, after which following becomes perfect ($\tilde{\mathcal{V}}_s = 1$). For Case 3, the highly polarized distribution becomes destabilized if it is not sufficiently aligned with the direction of the gradient, as occurs when the rotation becomes too fast to follow. The
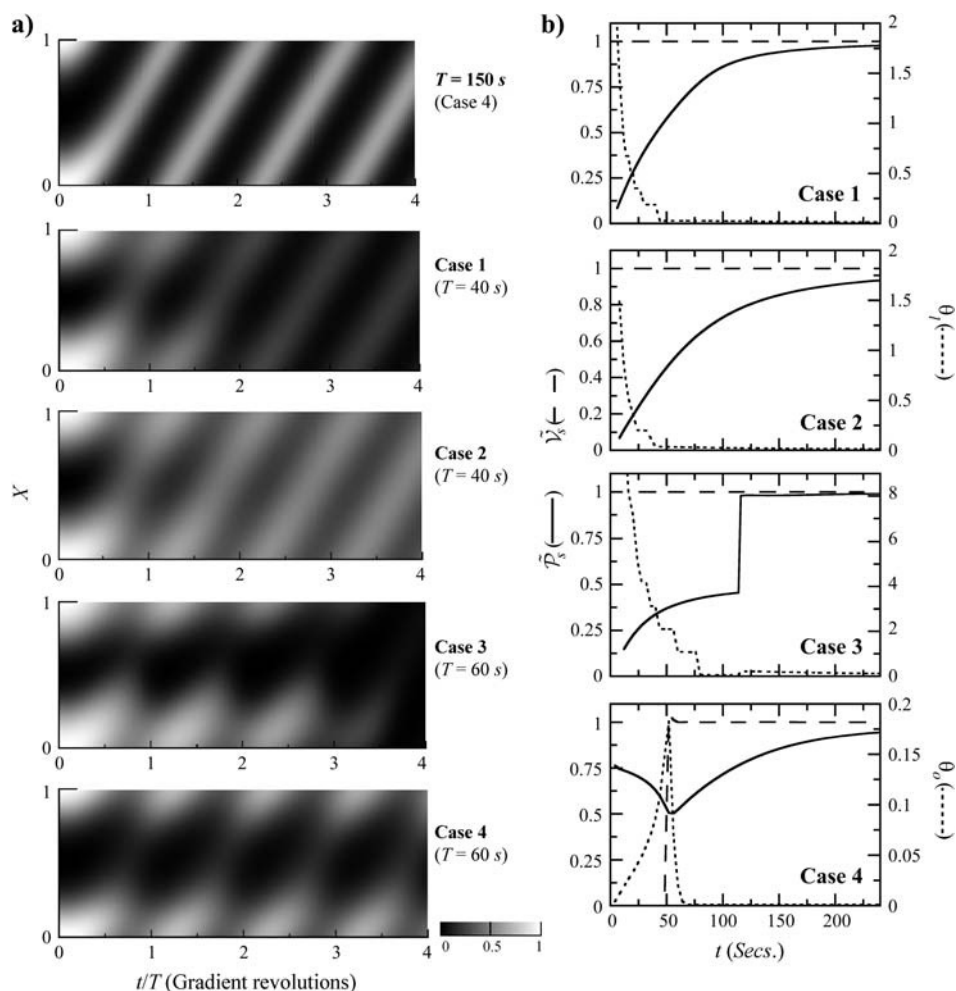
FIGURE 7 Responses to rotating gradients. Unstimulated cells are first polarized in a static gradient defined by $\mathcal{R} = S + G(1 + S)\cos(2\pi X)$, where $S = 2$ and $G = 0.075$. After cellular equilibration occurs, the gradient begins to rotate (at $t = 0$) and the stimulus is given by $\mathcal{R} = S + G(1 + S)\cos(2\pi(X - t/T))$, where T is the period of rotation. (*a*) Sample time courses of the P_n distribution are plotted as grayscale values, normalized by the peak P_n value before gradient rotation. The spatial variable X, is periodic, and t/T measures time in gradient rotations. $T = 150\ s$ (Case 4) illustrates efficient following of a slowly rotating gradient, as indicated by the steady diagonal translation of the grayscale pattern, with a period of 1 (responses for other cases were similar). (*b*) Quantities that characterize the response are recorded as a function of T. $\tilde{\mathcal{P}}_s$ and $\tilde{\mathcal{V}}_s$ are long-time averages of $\tilde{\mathcal{P}}(t) = \mathcal{P}\{P_n(t)\}/\mathcal{P}\{P_n(0)\}$ and $\tilde{\mathcal{V}}(t) = \mathcal{V}\{P_n(t)\}(T/2\pi)$, which represent normalized polarizations and angular velocities of the 3'PI distribution, respectively (see text and Eqs. 8–10). θ_L is the long-time value of $\theta\{P_n(t)\}/2\pi - t/T$ and measures the lag of the polarization angle behind that of the gradient for Cases 1–3; θ_o measures half the range of $\theta\{P_n(t)\}/2\pi - \tilde{\mathcal{V}}_s t/T$ during the time after oscillations become steady for Case 4; $\theta\{P_n(t)\}$ measures the direction of polarization of the P_n distribution (see Eq. 9).

sharp drop in $\tilde{\mathcal{P}}_s$ at shorter T is a discontinuity, and represents a bifurcation where the highly polarized distribution can no longer rotate stably at the frequency of gradient rotation; if the simulation is initialized in the weakly polarized state (that is, the gradient is applied without a sufficient uniform stimulus; see previous subsection), there is no discontinuity in the dose-response (not shown). Applying a weaker gradient resulted in destabilization of the highly polarized steady state at longer T, whereas a stronger gradient results in a highly polarized state that is stable at shorter T. For a sufficiently strong gradient, Case 3 no longer demonstrates a bistable response to static gradients (see Fig. 6 *b*), and responses to rotating gradients become similar to Case 1 (not shown). For Case 4, the polarized distribution remains stable when gradient rotation becomes too fast to follow, and an oscillatory motion results. The transition from gradient-following to oscillatory behavior occurs abruptly, and is indicated by the sharp drop in $\tilde{\mathcal{V}}_s$ at shorter T. Similar to Case 3, efficient gradient following continues at shorter T if a stronger gradient is used (not shown).

These simulations indicate that differences between our model variants are most apparent in the characteristics of transitions in response that occur when gradient rotation becomes too fast to follow. The observed differences do not imply that one variant functions more efficiently than the others; rather, each might have a different utility to any given cell types. In particular, these simulations demonstrate that under conditions where a bistable response is possible and the polarized response could potentially ''get stuck'' in an initial direction (as in Cases 3 and 4), the direction of polarization can still turn to follow a slowly rotating gradient. Although the simulations analyzed thus far are designed to probe the roles of coupled positive feedbacks and translocation in gradient sensing, we note that other types of dynamic simulations and experiments could be useful to further analyze our model, or to investigate other relevant biochemical/biophysical mechanisms (see, for example, Rappel et al. (19) and Subramanian and Narang (71)).

Defining criteria

We have already seen in Fig. 6 *b* that Cases 3 and 4 can be distinguished based on discontinuities in their dose-response curves to gradients, with possible dependence on application

of a uniform stimulus (differences are also clear in the dose-response curves to rotating gradients, as seen in Fig. 7 *b*). The distinct behaviors illustrated reflect the different roles played by coupled positive feedbacks in signal amplification. Comparison of the results in Figs. 5 *b* and 6 *b* suggests that in cases where translocation plays a significant role in stabilizing responses to gradients, a measure of the slope of the dose-response curve for gradients will be significantly greater than the slope for responses to uniform stimuli. Such a comparison is necessarily empirical and model dependent, as it requires accounting for the dynamic nature of responses to step stimuli, and for diffusive dissipation in responses to gradients. We formalize this comparison in Table 4. The given criteria distinguish between the four "modes" of gradient sensing, whose qualitative behaviors have been illustrated by the corresponding model variants.

Parameter space structure

To test whether the criteria in Table 4 can be applied to cells with unknown biochemical parameters, and to investigate the structure of our model's parameter space, we systematically varied two key parameters that had been used to specify our model variants: κ_K, which adjusts the effectiveness of Loop II in response amplification (see Eq. 3), and $1/\kappa_c$, which determines the degree to which cytoplasmic depletion in Loop I saturates the amplification module (see Eqs. 1 and 1a). For each combination of κ_K and κ_c, γ_0 was chosen to optimize the polarization of the 3'PI distribution in response to a small gradient, as our analysis in Fig. 4 *b* had suggested that this is important for efficient gradient sensing. All other parameters were fixed at the values used in previous simulations (given in Table 2 and Supplementary Material).

For each combination of parameters, we generated dose-response curves to uniform stimuli and to gradients applied together with, and after equilibration to, a uniform stimulus. The criteria in Table 4 were applied. The results are sum-marized in Fig. 8 *a*, where the numbers label regions on this surface in parameter space according to the mode of gradient sensing that best characterizes the simulated responses. An asterisk (*) in a region marks the combination of parameters used to define the corresponding model variant. Regions that gave ambiguous results with respect to translocation were labeled 3′ or 4′ if they met criteria for Modes 3 or 4 with respect to coupled positive feedbacks, and 1′/2′ otherwise (our criteria relating to coupled positive feedbacks alone do not distinguish between Cases 1 and 2). If the relative polarization in response to a gradient defined by $G = 0.05$ was <0.4 (about half the average value calculated for our model variants; see Fig. 6 *b*), the region was labeled as "weakly polarized". We also simulated responses to a rotating gradient with a period of 150 s. Regions were labeled as "poorly following" if either the steady normalized polarization or angular velocity was below 0.6 (see Fig. 7). In these regions of inefficient gradient sensing, we did not apply our criteria.

In Fig. 8 *a*, we see that decreasing κ_K (which increases the effectiveness of Loop II) leads to transitions to modes with successively higher gain in response. For example, decreasing κ_K at $1/\kappa_c = 0.5$ results in the sequence of transitions: 'Weakly polarized' → Mode 2 → Mode 4 → Mode 4′ → Mode 3′ → 'Poorly following'. Increasing $1/\kappa_c$ leads to transition to modes where redistribution of translocating molecules makes coupled positive feedbacks more effective in responses to gradients. For example, decreasing $1/\kappa_c$ at $\kappa_K = 3$ results in the sequence of transitions: 'Weakly polarized' → Mode 1′/2′ → Mode 2 → Mode 4. In general, transitions between modes that differ in the roles played by coupled positive feedbacks are sharp (indicated by a *bold line*), whereas transitions between modes that differ in the importance of translocation pass through regions of parameter space whose qualitative behavior is ambiguous (labeled 1′/2′, 3′, or 4′). Further, the regions where each variant functions efficiently might be narrow in some directions, suggesting constraints on parameters.

The qualitative results of varying other model parameters can be similarly understood, based on the degree to which they adjust the strength of positive feedbacks and the importance of translocating molecules in our model. As an example, we have varied the parameter ζ_T in Eq. 4. This adjusts the importance of constitutive removal of PTEN from the membrane. Larger ζ_T means a less significant inverse translocation of PTEN from the membrane in response to external stimuli, making Loop II less effective. Beginning with the set of parameters that defines Case 1, ζ_T and $1/\kappa_c$ were varied to generate Fig. 8 *b*, in the same way that Fig. 8 *a* was generated. To maintain a similar baseline value of T_m when ζ_T was varied, λ_T was adjusted such that $\lambda_T(K_{m1} + \zeta_T) = $ constant, where K_{m1} is the value of K_m in the unstimulated cell for Case 1.

Comparing the structures in Fig. 8, *a* and *b*, we see that similar transitions result when κ_K is decreased (panel *a*) or

TABLE 4 Criteria for distinguishing modes of gradient sensing

	Mode 1	Mode 2	Mode 3	Mode 4
Relating to coupled positive feedbacks:				
Discontinuity in dose-response to gradients	No	No	Yes	Yes
Dependence of gradient dose-response on simultaneous application of a uniform stimulus	No	No	Yes	No
Relating to translocation:				
Responses to uniform stimuli comparable to responses to gradients*	Yes	No	Yes	No

*We consider responses to uniform stimuli and to gradient stimuli to be comparable if $G\big[(\partial)/\partial S(P_n)_{\text{max}}\big]_{\text{max}} > 0.4\mathcal{P}\{G\}$, not comparable if $G\big[(\partial)/\partial S(P_n)_{\text{max}}\big]_{\text{max}} < 0.2\mathcal{P}\{G\}$, and ambiguous otherwise. S specifies a uniform stimulus and $(P_n)_{\text{max}}$ quantifies the peak response, as in Fig. 5; G specifies a gradient stimulus, and $\mathcal{P}\{G\}$ quantifies the polarized response, as in Fig. 6. $G = 0.05$ was used.
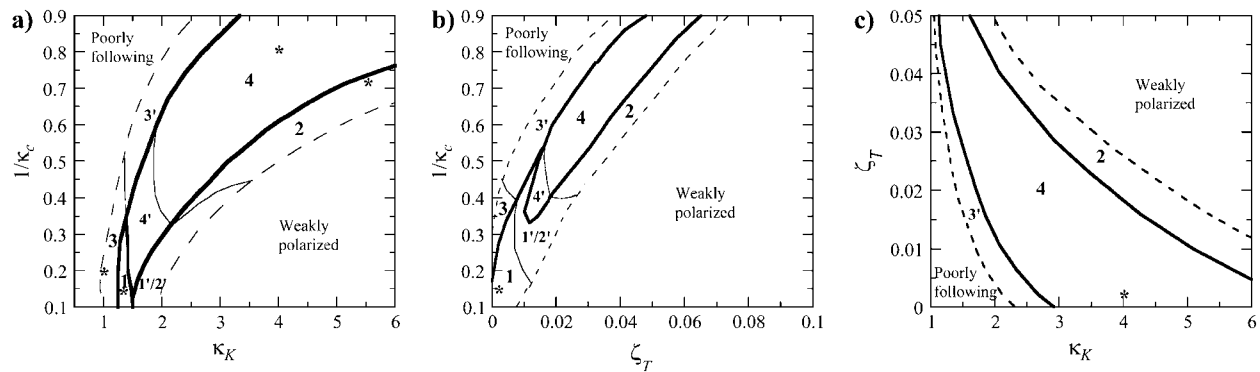
FIGURE 8   Partitioning of parameter space. Parameters affecting the roles of coupled positive feedbacks and translocation are varied. Criteria in Table 4 are applied to simulation results, as described in the text, and regions of parameter space are labeled by the mode of gradient sensing that best characterizes the results. An asterisk (*) in a region labels parameter values used to define the corresponding model variant. Regions where results are ambiguous with respect to translocation are labeled $3'$ or $4'$ if they meet criteria for Modes 3 or 4 with respect to coupled positive feedbacks, and $1'/2'$ otherwise. Bold lines mark bifurcations, and separate behaviors with different steady-state properties. Dashed lines separate regions of efficient and inefficient gradient sensing. (*a*) κ_K and κ_c, are varied. Decreased κ_K means that feedback in Loop II is more effective; increased $1/\kappa_c$ means that translocation is more significant in amplifying responses to gradients. (*b*) $1/\kappa_c$ and ζ_T are varied, starting with the combination of parameters used to define Case 1, as described in the text. Greater ζ_T means that PTEN translocation in response to outside stimuli is less significant and the feedback in Loop II is weakened. (*c*) ζ_T and κ_K are varied, starting with the set of parameters used to define Case 4. Increasing ζ_T can be compensated for by appropriately decreasing κ_K.

when ζ_T is decreased (panel *b*). Thus, we might expect that their simultaneous variations can compensate for each other. This is demonstrated in Fig. 8 *c*, where we see that decreasing κ_K while appropriately increasing ζ_T often result in the same mode of gradient sensing (other parameters were set as in Case 4). Similar results were found for variations of other parameters, such as κ_3, which adjusts the value of K_m for which binding of PI3K to the PITP becomes saturated (results not shown).

SUMMARY AND DISCUSSION

We have developed a model of eukaryotic gradient sensing at an intermediate level of detail. The model is based on a scheme of $3'$PI signaling thought to be important in chemotaxis of highly motile cells such as *Dictyostelium* and neutrophils. By appropriately adjusting parameters, we defined and analyzed four variants of our model, whose qualitative features are summarized in Table 3. Our variants differ in whether coupled positive feedbacks lead to multiple steady states, and whether redistribution of molecules that translocate from the cytosol to the membrane leads to significant differences in responses to uniform stimuli and to gradients. We expect these possibilities to be available to any gradient sensing cell.

Each of our model variants accounts for the characteristic behaviors of gradient sensing enumerated in our Introduction. Experimentally, these are generally elicited by strong stimuli, such as a saturating uniform dose of chemoattractant, or a steep gradient (e.g., generated by a pipette that leaks chemoattractant close to the cell). Our simulations suggest that each variant behaves differently under conditions where the gradient sensing response begins to fail. For example: when a uniform stimulus becomes too small to elicit an ob-

servable response; when a gradient is too small to produce a highly polarized response; or when the pipette in a rotating gradient experiment begins to move too quickly for the cell to follow. These transitions, from efficient gradient detection to failure, are best observed in dose-response experiments (Figs. 5–7).

Based on differences in simulated dose-response experiments to uniform stimuli and to gradients of different strengths (Figs. 5 and 6), we have defined criteria that determine whether a cell with unknown biochemical parameters makes use of a mode of gradient sensing illustrated by one of our model variants (Table 4). Using these criteria, we have characterized several surfaces in the parameter space of our model by determining which mode of gradient sensing best describes the behavior at each point (Fig. 8). Because our criteria depend on qualitative differences in response, rather than particular details of our model, we expect them to be applicable as well to other gradient sensing cells that display characteristic behaviors, and to analyzing models based on other biochemical schemes.

Our analysis of cellular response to rotating gradients (Fig. 7) suggests that the differences that define our variants have consequences for cellular behaviors in natural settings, where chemotactic stimuli vary in both space and time. For example, Cases 1 and 2 always follow a rotating gradient perfectly, their polarization gradually weakening for fast rotations. The polarized response for Case 3 can be turned on and off by strong stimuli that change quickly. Case 4 remains persistently polarized in an initial direction when the gradient changes quickly. Each type of behavior might have a different utility for the cells that use them. These differences would influence, for example, the patterns formed during *Dictyostelium* aggregation, and the population dynamics of neutrophils migrating to a source of infection.

Applying the criteria in Table 4 to real cells could guide the identification of important positive feedbacks and trans-locating molecules that shape essential features of gradient sensing responses; our model could be used to suggest the qualitative results of perturbing these elements. For such applications, cell to cell variability will have important consequences. The values of biochemical parameters in each cell, even in a clonal population, will generally be different (different concentrations of each protein will be expressed, etc.). Responses to a given stimulus will then vary, and transitions in the response of a given cell will occur at different stimuli. Thus, multiple experiments must be done on single cells to apply the criteria in Table 4, and analysis of many cells will be necessary to characterize the distribution of behaviors in a population. The need for quantitative measurements on single cells to observe transitions in behavior has been emphasized in connection to other cellular systems (see, for example, Cluzel et al. (72) and Ferrell and Machleder (73)); such measurements are only recently being done in connection to gradient sensing (for example, Postma et al. and others (15,17,35,74).

In developing our model, we found that many parameter variations had similar effects and could compensate for each other. Further, certain combinations of parameters were more important than others in determining qualitative behaviors. For example, varying any of the several parameters that control the strength of the positive feedbacks in our model might lead to similar bifurcations. This is illustrated in Fig. 8, where the boundaries that separate Cases 1 and 2 (which have unique steady states) from Cases 3 and 4 (which have multiple steady states) are highlighted in bold. Combinations of parameters near these boundaries often resulted in more efficient gradient sensing responses. For example, Modes 1 and 2 showed enhanced responses to small gradients; Modes 3 and 4 followed rotating gradients more efficiently. As with our analysis of constraints in Fig. 4, these observations suggest that some combinations of parameters must be set quite carefully for efficient gradient sensing, and that homeostatic mechanisms exist to maintain their balance in cells.

The partitioning illustrated in Fig. 8 suggests that we think of the different modes of gradient sensing, represented by our model variants, as existing within volumes of parameter space and functioning efficiently within subvolumes. These subvolumes might have sharp boundaries and may be narrow with respect to variations of some combinations of parameters. This presents the intriguing possibility that different cells in a population, which differ in the values of their biochemical parameters, might employ different modes of gradient sensing and function at varying levels of efficiency. Each mode may have a different utility to a cell of a given type. Thus, during the course of development, a cell might transition between efficient gradient detection and nonresponsiveness, or between different modes of gradient detection, by modulating its biochemical parameters to suit its needs.

SUPPLEMENTARY MATERIAL

An online supplement to this article can be found by visiting BJ Online at http://www.biophysj.org.

REFERENCES

1. Yang, X., D. Dormann, A. E. Munsterberg, and C. J. Weijer. 2002. Cell movement patterns during gastrulation in the chick are controlled by positive and negative chemotaxis mediated by FGF4 and FGF8. *Dev. Cell.* 3:425–437.

2. Zeller, P. J., T. C. Skalak, A. M. Ponce, and R. J. Price. 2001. In vivo chemotactic properties and spatial expression of PDGF in developing mesenteric microvascular networks. *Am. J. Physiol. Heart Circ. Physiol.* 280:H2116–H2125.

3. Isbister, C. M., P. J. Mackenzie, K. C. To, and T. P. O'Connor. 2003. Gradient steepness influences the pathfinding decisions of neuronal growth cones in vivo. *J. Neurosci.* 23:193–202.

4. Gillitzer, R., and M. Goebeler. 2001. Chemokines in cutaneous wound healing. *J. Leukoc. Biol.* 69:513–521.

5. Olson, T. S., and K. Ley. 2002. Chemokines and chemokine receptors in leukocyte trafficking. *Am. J. Physiol. Regul. Integr. Comp. Physiol.* 283:R7–28.

6. Firtel, R. A., and R. Meili. 2000. Dictyostelium: a model for regulated cell movement during morphogenesis. *Curr. Opin. Genet. Dev.* 10:421–427.

7. Devreotes, P., and C. Janetopoulos. 2003. Eukaryotic chemotaxis: distinctions between directional sensing and polarization. *J. Biol. Chem.* 278:20445–20448.

8. Zigmond, S. H., H. I. Levitsky, and B. J. Kreel. 1981. Cell polarity: an examination of its behavioral expression and its consequences for polymorphonuclear leukocyte chemotaxis. *J. Cell Biol.* 89:585–592.

9. Fisher, P. R., R. Merkl, and G. Gerisch. 1989. Quantitative analysis of cell motility and chemotaxis in Dictyostelium discoideum by using an image processing system and a novel chemotaxis chamber providing stationary chemical gradients. *J. Cell Biol.* 108:973–984.

10. Iijima, M., Y. E. Huang, and P. Devreotes. 2002. Temporal and spatial regulation of chemotaxis. *Dev. Cell.* 3:469–478.

11. Weiner, O. D. 2002. Regulation of cell polarity during eukaryotic chemotaxis: the chemotactic compass. *Curr. Opin. Cell Biol.* 14:196–202.

12. Kam, J. L., K. Miura, T. R. Jackson, J. Gruschus, P. Roller, S. Stauffer, J. Clark, R. Aneja, and P. A. Randazzo. 2000. Phosphoinositide-dependent activation of the ADP-ribosylation factor GTPase-activating protein ASAP1. Evidence for the pleckstrin homology domain functioning as an allosteric site. *J. Biol. Chem.* 275:9653–9663.

13. Yin, H. L., and P. A. Janmey. 2003. Phosphoinositide regulation of the actin cytoskeleton. *Annu. Rev. Physiol.* 65:761–789.

14. Chen, L., C. Janetopoulos, Y. E. Huang, M. Iijima, J. Borleis, and P. N. Devreotes. 2003. Two phases of actin polymerization display different dependencies on PI(3,4,5)P3 accumulation and have unique roles during chemotaxis. *Mol. Biol. Cell.* 14:5028–5037.

15. Postma, M., J. Roelofs, J. Goedhart, H. M. Loovers, A. J. Visser, and P. J. Van Haastert. 2004. Sensitization of Dictyostelium chemotaxis by phosphoinositide-3-kinase-mediated self-organizing signalling patches. *J. Cell Sci.* 117:2925–2935.

16. Srinivasan, S., F. Wang, S. Glavas, A. Ott, F. Hofmann, K. Aktories, D. Kalman, and H. R. Bourne. 2003. Rac and Cdc42 play distinct roles

in regulating PI(3,4,5)P3 and polarity during neutrophil chemotaxis. *J. Cell Biol.* 160:375–385.

17. Janetopoulos, C., L. Ma, P. N. Devreotes, and P. A. Iglesias. 2004. Chemoattractant-induced phosphatidylinositol 3,4,5-trisphosphate accumulation is spatially amplified and adapts, independent of the actin cytoskeleton. *Proc. Natl. Acad. Sci. USA.* 101:8951–8956.

18. Jin, T., N. Zhang, Y. Long, C. A. Parent, and P. N. Devreotes. 2000. Localization of the G protein betagamma complex in living cells during chemotaxis. *Science.* 287:1034–1036.

19. Rappel, W. J., P. J. Thomas, H. Levine, and W. F. Loomis. 2002. Establishing direction during chemotaxis in eukaryotic cells. *Biophys. J.* 83:1361–1367.

20. Haugh, J. M., and I. C. Schneider. 2004. Spatial analysis of 3′ phosphoinositide signaling in living fibroblasts. I. Uniform stimulation model and bounds on dimensionless groups. *Biophys. J.* 86:589–598.

21. Levchenko, A., and P. A. Iglesias. 2002. Models of eukaryotic gradient sensing: application to chemotaxis of amoebae and neutrophils. *Biophys. J.* 82:50–63.

22. Narang, A., K. K. Subramanian, and D. A. Lauffenburger. 2001. A mathematical model for chemoattractant gradient sensing based on receptor-regulated membrane phospholipid signaling dynamics. *Ann. Biomed. Eng.* 29:677–691.

23. Postma, M., and P. J. Van Haastert. 2001. A diffusion-translocation model for gradient sensing by chemotactic cells. *Biophys. J.* 81:1314–1323.

24. Iglesias, P. A., and A. Levchenko. 2002. Modeling the cell's guidance system. *Sci. STKE.* 2002:RE12.

25. Zigmond, S. H. 1977. Ability of polymorphonuclear leukocytes to orient in gradients of chemotactic factors. *J. Cell Biol.* 75:606–616.

26. Parent, C. A., B. J. Blacklock, W. M. Froehlich, D. B. Murphy, and P. N. Devreotes. 1998. G protein signaling events are activated at the leading edge of chemotactic cells. *Cell.* 95:81–91.

27. Servant, G., O. D. Weiner, P. Herzmark, T. Balla, J. W. Sedat, and H. R. Bourne. 2000. Polarization of chemoattractant receptor signaling during neutrophil chemotaxis. *Science.* 287:1037–1040.

28. Meinhardt, H., and A. Gierer. 2000. Pattern formation by local self-activation and lateral inhibition. *Bioessays.* 22:753–760.

29. Gierer, A., and H. Meinhardt. 1972. A theory of biological pattern formation. *Kybernetik.* 12:30–39.

30. Meinhardt, H. 1999. Orientation of chemotactic cells and growth cones: models and mechanisms. *J. Cell Sci.* 112:2867–2874.

31. Devreotes, P. N., and S. H. Zigmond. 1988. Chemotaxis in eukaryotic cells: a focus on leukocytes and Dictyostelium. *Annu. Rev. Cell Biol.* 4:649–686.

32. Parent, C. A., and P. N. Devreotes. 1999. A cell's sense of direction. *Science.* 284:765–770.

33. Ruchira, M., A. Hink, L. Bosgraaf, P. J. van Haastert, and A. J. Visser. 2004. Pleckstrin homology domain diffusion in Dictyostelium cytoplasm studied using fluorescence correlation spectroscopy. *J. Biol. Chem.* 279:10013–10019.

34. Ueda, M., Y. Sako, T. Tanaka, P. Devreotes, and T. Yanagida. 2001. Single-molecule analysis of chemotactic signaling in Dictyostelium cells. *Science.* 294:864–867.

35. Schneider, I. C., and J. M. Haugh. 2004. Spatial analysis of 3′ phosphoinositide signaling in living fibroblasts. II. Parameter estimates for individual cells from experiments. *Biophys. J.* 86:599–608.

36. Servant, G., O. D. Weiner, E. R. Neptune, J. W. Sedat, and H. R. Bourne. 1999. Dynamics of a chemoattractant receptor in living neutrophils during chemotaxis. *Mol. Biol. Cell.* 10:1163–1178.

37. Funamoto, S., R. Meili, S. Lee, L. Parry, and R. A. Firtel. 2002. Spatial and temporal regulation of 3-phosphoinositides by PI 3-kinase and PTEN mediates chemotaxis. *Cell.* 109:611–623.

38. Brock, C., M. Schaefer, H. P. Reusch, C. Czupalla, M. Michalke, K. Spicher, G. Schultz, and B. Nurnberg. 2003. Roles of G beta gamma in membrane recruitment and activation of p110 gamma/p101 phosphoinositide 3-kinase gamma. *J. Cell Biol.* 160:89–99.

39. Janetopoulos, C., T. Jin, and P. Devreotes. 2001. Receptor-mediated activation of heterotrimeric G-proteins in living cells. *Science.* 291:2408–2411.

40. Vanhaesebroeck, B., S. J. Leevers, K. Ahmadi, J. Timms, R. Katso, P. C. Driscoll, R. Woscholski, P. J. Parker, and M. D. Waterfield. 2001. Synthesis and function of 3-phosphorylated inositol lipids. *Annu. Rev. Biochem.* 70:535–602.

41. Rickert, P., O. D. Weiner, F. Wang, H. R. Bourne, and G. Servant. 2000. Leukocytes navigate by compass: roles of PI3Kgamma and its lipid products. *Trends Cell Biol.* 10:466–473.

42. Chung, C. Y., S. Funamoto, and R. A. Firtel. 2001. Signaling pathways controlling cell polarity and chemotaxis. *Trends Biochem. Sci.* 26:557–566.

43. Backers, K., D. Blero, N. Paternotte, J. Zhang, and C. Erneux. 2003. The termination of PI3K signalling by SHIP1 and SHIP2 inositol 5-phosphatases. *Adv. Enzyme Regul.* 43:15–28.

44. Weiner, O. D., P. O. Neilsen, G. D. Prestwich, M. W. Kirschner, L. C. Cantley, and H. R. Bourne. 2002. A PtdInsP(3)- and Rho GTPase-mediated positive feedback loop regulates neutrophil polarity. *Nat. Cell Biol.* 4:509–513.

45. Skippen, A., D. H. Jones, C. P. Morgan, M. Li, and S. Cockcroft. 2002. Mechanism of ADP ribosylation factor-stimulated phosphatidylinositol 4,5-bisphosphate synthesis in HL60 cells. *J. Biol. Chem.* 277:5823–5831.

46. Weernink, P. A., K. Meletiadis, S. Hommeltenberg, M. Hinz, H. Ishihara, M. Schmidt, and K. H. Jakobs. 2004. Activation of type I phosphatidylinositol 4-phosphate 5-kinase isoforms by the Rho GTPases, RhoA, Rac1, and Cdc42. *J. Biol. Chem.* 279:7840–7849.

47. Stephens, L. R., K. T. Hughes, and R. F. Irvine. 1991. Pathway of phosphatidylinositol(3,4,5)-trisphosphate synthesis in activated neutrophils. *Nature.* 351:33–39.

48. Huang, Y. E., M. Iijima, C. A. Parent, S. Funamoto, R. A. Firtel, and P. Devreotes. 2003. Receptor-mediated regulation of PI3Ks confines PI(3,4,5)P3 to the leading edge of chemotaxing cells. *Mol. Biol. Cell.* 14:1913–1922.

49. Iijima, M., and P. Devreotes. 2002. Tumor suppressor PTEN mediates sensing of chemoattractant gradients. *Cell.* 109:599–610.

50. Yi, T. M., Y. Huang, M. I. Simon, and J. Doyle. 2000. Robust perfect adaptation in bacterial chemotaxis through integral feedback control. *Proc. Natl. Acad. Sci. USA.* 97:4649–4653.

51. Czupalla, C., M. Culo, E. C. Muller, C. Brock, H. P. Reusch, K. Spicher, E. Krause, and B. Nurnberg. 2003. Identification and characterization of the autophosphorylation sites of phosphoinositide 3-kinase isoforms beta and gamma. *J. Biol. Chem.* 278:11536–11545.

52. Vazquez, F., S. Ramaswamy, N. Nakamura, and W. R. Sellers. 2000. Phosphorylation of the PTEN tail regulates protein stability and function. *Mol. Cell. Biol.* 20:5010–5018.

53. Jackson, T. R., B. G. Kearns, and A. B. Theibert. 2000. Cytohesins and centaurins: mediators of PI 3-kinase-regulated Arf signaling. *Trends Biochem. Sci.* 25:489–495.

54. Welch, H. C., W. J. Coadwell, L. R. Stephens, and P. T. Hawkins. 2003. Phosphoinositide 3-kinase-dependent activation of Rac. *FEBS Lett.* 546:93–97.

55. Hawadle, M. A., N. Folarin, R. Martin, and T. R. Jackson. 2002. Cytohesins and centaurins control subcellular trafficking of macromolecular signaling complexes: regulation by phosphoinositides and ADP-ribosylation factors. *Biol. Res.* 35:247–265.

56. Ridley, A. J. 2001. Rho GTPases and cell migration. *J. Cell Sci.* 114:2713–2722.

57. Xu, J., F. Wang, A. Van Keymeulen, P. Herzmark, A. Straight, K. Kelly, Y. Takuwa, N. Sugimoto, T. Mitchison, and H. R. Bourne. 2003. Divergent signals and cytoskeletal assemblies regulate self-organizing polarity in neutrophils. *Cell.* 114:201–214.

58. Glogauer, M., J. Hartwig, and T. Stossel. 2000. Two pathways through Cdc42 couple the N-formyl receptor to actin nucleation in permeabilized human neutrophils. *J. Cell Biol.* 150:785–796.

59. Randazzo, P. A., and D. S. Hirsch. 2004. Arf GAPs: multifunctional proteins that regulate membrane traffic and actin remodelling. *Cell. Signal.* 16:401–413.

60. Insall, R. H., and O. D. Weiner. 2001. PIP3, PIP2, and cell movement–similar messages, different meanings? *Dev. Cell.* 1:743–747.

61. Stauffer, T. P., S. Ahn, and T. Meyer. 1998. Receptor-induced transient reduction in plasma membrane PtdIns(4,5)P2 concentration monitored in living cells. *Curr. Biol.* 8:343–346.

62. Kular, G., M. Loubtchenkov, P. Swigart, J. Whatmore, A. Ball, S. Cockcroft, and R. Wetzker. 1997. Co-operation of phosphatidylinositol transfer protein with phosphoinositide 3-kinase gamma in the formylmethionyl-leucylphenylalanine-dependent production of phosphatidylinositol 3,4,5-trisphosphate in human neutrophils. *Biochem. J.* 325:299–301.

63. Li, Z., H. Jiang, W. Xie, Z. Zhang, A. V. Smrcka, and D. Wu. 2000. Roles of PLC-beta2 and -beta3 and PI3Kgamma in chemoattractant-mediated signal transduction. *Science.* 287:1046–1049.

64. Bondeva, T., L. Pirola, G. Bulgarelli-Leva, I. Rubio, R. Wetzker, and M. P. Wymann. 1998. Bifurcation of lipid and protein kinase signals of PI3Kgamma to the protein kinases PKB and MAPK. *Science.* 282: 293–296.

65. Vanhaesebroeck, B., K. Higashi, C. Raven, M. Welham, S. Anderson, P. Brennan, S. G. Ward, and M. D. Waterfield. 1999. Autophosphorylation of p110delta phosphoinositide 3-kinase: a new paradigm for the regulation of lipid kinases in vitro and in vivo. *EMBO J.* 18:1292–1302.

66. Iijima, M., Y. E. Huang, H. R. Luo, F. Vazquez, and P. N. Devreotes. 2004. Novel mechanism of PTEN regulation by its phosphatidylinositol 4,5-bisphosphate binding motif is critical for chemotaxis. *J. Biol. Chem.* 279:16606–16613.

67. Rhee, S. G. 2001. Regulation of phosphoinositide-specific phospholipase C. *Annu. Rev. Biochem.* 70:281–312.

68. McConnachie, G., I. Pass, S. M. Walker, and C. P. Downes. 2003. Interfacial kinetic analysis of the tumour suppressor phosphatase, PTEN: evidence for activation by anionic phospholipids. *Biochem. J.* 371:947–955.

69. Ma, L., C. J. Janetopoulos, L. Yang, P. N. Devreotes, and P. A. Iglesias. 2004. Two local excitation, global inhibition mechanisms acting complementarily in parallel can explain the chemoattractant-induced PI(3,4,5)P3 response in Dictyostelium. *Biophys. J.* 87:3764–3774.

70. Press, W. H., S. A. Teukolsky, W. T. Vettering, and B. P. Flannery. 2002. Numerical Recipes in C: The Art of Scientific Computing. Cambridge University Press, Cambridge (Cambridgeshire), UK; New York, NY.

71. Subramanian, K. K., and A. Narang. 2004. A mechanistic model for eukaryotic gradient sensing: spontaneous and induced phosphoinositide polarization. *J. Theor. Biol.* 231:49–67.

72. Cluzel, P., M. Surette, and S. Leibler. 2000. An ultrasensitive bacterial motor revealed by monitoring signaling proteins in single cells. *Science.* 287:1652–1655.

73. Ferrell, J. E., Jr., and E. M. Machleder. 1998. The biochemical basis of an all-or-none cell fate switch in Xenopus oocytes. *Science.* 280:895–898.

74. Xu, X., M. Meier-Schellersheim, X. Jiao, L. E. Nelson, and T. Jin. 2004. Quantitative imaging of single live cells reveals spatiotemporal dynamics of multi-step signaling events of chemoattractant gradient sensing in Dictyostelium. *Mol. Biol. Cell.* 16:676–688.